

Article

Not peer-reviewed version

S-ResGCN: A Symmetry-Aware Graph Convolutional Network for MRI-Based Brain Tumor Diagnosis

[Yingzhou Bi](#)*, [Qiujiang Gan](#), [Leigang Huo](#), [Shanrui Liu](#), [Kairui Xiong](#)

Posted Date: 1 October 2025

doi: 10.20944/preprints202510.0008.v1

Keywords: MRI; brain tumor; symmetry; ResNet18; adaptive convolution; multi-level attention modules; spatial-aware convolution





Preprints.org is a free multidisciplinary platform providing preprint service that is dedicated to making early versions of research outputs permanently available and citable. Preprints posted at Preprints.org appear in Web of Science, Crossref, Google Scholar, Scilit, Europe PMC.

Copyright: This open access article is published under a Creative Commons CC BY 4.0 license, which permit the free download, distribution, and reuse, provided that the author and preprint are cited in any reuse.

Disclaimer/Publisher's Note: The statements, opinions, and data contained in all publications are solely those of the individual author(s) and contributor(s) and not of MDPI and/or the editor(s). MDPI and/or the editor(s) disclaim responsibility for any injury to people or property resulting from any ideas, methods, instructions, or products referred to in the content.

Article

S-ResGCN: A Symmetry-Aware Graph Convolutional Network for MRI-Based Brain Tumor Diagnosis

Yingzhou Bi , Qiujiang Gan , Leigang Huo , Shanrui Liu, and Kairui Xiong

School of Artificial Intelligence, Nanning Normal University, Nanning 530199, China

* Correspondence: xxjs@nnnu.edu.cn (Y.B.)

Abstract

Early and accurate detection of brain tumors is critical for MRI-based diagnosis. Conventional convolutional neural networks often struggle to capture fine-grained details, small or boundary-ambiguous lesions, and hemispheric symmetry patterns. To address these limitations, we propose S-ResGCN, a symmetry-aware framework integrating hierarchical feature extraction, attention mechanisms, and graph-based classification. S-ResGCN employs a ResNet50 backbone to extract multi-level features, with Convolutional Block Attention Modules applied to intermediate and deep layers to enhance key information and discriminative features. Furthermore, we introduce a novel self-paired regularization to enforce feature consistency between original and horizontally flipped images, improving sensitivity to bilateral symmetric structures. Extracted features are converted into nodes and modeled as a small graph, and a graph convolutional network captures inter-node relationships to generate symmetry-aware predictions. Evaluation on two publicly available brain tumor MRI datasets demonstrates that S-ResGCN achieves average accuracies of 99.83% and 99.37%, with consistently high precision, recall, and F1-scores. These results indicate that S-ResGCN effectively captures fine-grained and symmetric tumor characteristics often overlooked by conventional models, providing a robust and efficient tool for automated, symmetry-aware brain tumor diagnosis.

Keywords: MRI; brain tumor; symmetry; ResNet18; adaptive convolution; multi-level attention modules; spatial-aware convolution

1. Introduction

Brain tumors are among the most common and aggressive malignancies of the central nervous system, typically arising from the abnormal proliferation of glial or meningeal cells. They pose a severe threat to neurological function and patient survival. Epidemiological studies indicate that brain tumors rank among the leading causes of mortality and disability in neurological disorders, particularly when lesions occur in critical brain regions where they can profoundly impair speech, motor, and cognitive functions. In addition to their heterogeneous and irregular morphologies, brain tumors often exhibit locally symmetric growth patterns, which complicates accurate identification and precise boundary delineation. Consequently, early detection and timely intervention are essential for improving survival rates, delaying disease progression, and optimizing patient outcomes. Prompt tumor identification not only reduces surgical risks but also prevents irreversible neurological damage.

Magnetic resonance imaging (MRI) [1], with its superior soft-tissue contrast, non-ionizing nature, and multi-sequence imaging capability, has become an indispensable modality for clinical brain tumor diagnosis. MRI enables clear visualization of abnormal brain structures, providing reliable evidence for tumor detection, localization, and grading. However, the interpretation of MRI scans is highly dependent on radiologists' expertise and subjective judgment. This dependence can prolong diagnostic time and introduce variability due to differences in clinical experience or visual fatigue, ultimately reducing diagnostic consistency and accuracy. To address these challenges, traditional computer-aided diagnosis (CAD) [2] methods have been extensively applied to brain MRI analysis. Such approaches

rely on handcrafted feature extraction—commonly including texture descriptors (e.g., gray-level co-occurrence matrices, local binary patterns), shape features, and statistical measures—followed by classification using machine learning algorithms such as support vector machines (SVM) [3], random forests (RF) [4], or k-nearest neighbors (KNN) [5]. Although these methods achieved early success, their labor-intensive feature engineering, subjectivity, and limited generalization ability hinder their effectiveness for the complex, diverse, and locally symmetric morphological characteristics of brain tumors.

In recent years, deep learning has emerged as the dominant paradigm for medical image analysis, with convolutional neural networks (CNNs) [6] demonstrating remarkable performance in brain tumor classification tasks. For example, Musa et al. [7] constructed a ResNet50-based detection model that effectively assisted radiologists in identifying abnormal regions and improving diagnostic accuracy. Khan et al. [8] proposed an optimized CNN architecture that significantly enhanced classification performance while maintaining manageable model complexity. Other studies have incorporated pre-trained networks to improve generalization; Nizamli et al. [9] used a fixed-weight VGG-19 network to convert MRI images into high-level feature representations combined with an SVM classifier, achieving shorter training times without compromising accuracy. Similarly, Haq et al. [10] integrated CNNs with long short-term memory networks to capture both spatial and temporal information, further improving performance through data augmentation. However, these approaches often rely heavily on global features and fail to explicitly capture fine local details and symmetry-related structures, resulting in reduced sensitivity to small, blurred, or irregular lesions—critical for precise clinical diagnosis.

To design deep learning architectures that are robust and sensitive to local symmetry, insights from graph theory and complex network analysis can be particularly valuable. Previous studies—such as those by Wang et al. [11], Wang et al. [12,13] and Jiang et al. [14]—have systematically investigated the connectivity and diagnosability of locally twisted cubes, leaf-sort graphs, and maximally 4-restricted edge-connected graphs. Additionally, the connectivity and diagnosability of leaf-sort graphs were further explored in a separate study by Wang et al. [15]. The maximum forcing number of polyominoes was reported by Lin et al. [16], and the connectivity of m-ary n-dimensional hypercubes was investigated in [17]. These studies highlight the importance of information-flow reliability, fault tolerance, and node-level symmetry in complex networks, providing a conceptual foundation for developing deep learning architectures capable of capturing local structural and symmetric patterns in brain MRI.

Motivated by these considerations, we propose S-ResGCN, a symmetry-aware framework for brain tumor classification. S-ResGCN adopts a ResNet50 backbone to extract hierarchical feature representations, with Convolutional Block Attention Modules (CBAM) [18] applied to intermediate and deep layers to enhance key information and discriminative features. Inspired by consistency regularization approaches [19], we introduce a novel self-paired regularization (SPR) loss specifically designed to enforce feature consistency between original and horizontally flipped images, thereby improving the model's sensitivity to bilateral structures. Node features are constructed via global average pooling of the original and flipped feature maps and modeled as a small graph. A graph convolutional network (GCN) [20] head captures inter-node relationships, and aggregated node outputs yield symmetry-aware predictions. This architecture enables robust detection of complex and symmetric lesions, improving classification performance for brain tumor MRI.

2. Materials and Methods

2.1. Dataset

We retrospectively collected a total of 7,023 MRI images from the Brain Tumor MRI Dataset [21] and 3,264 MRI images from the Brain Tumor MRI Dataset [22]. As shown in Figure 1, both datasets encompass four tumor categories. Dataset I comprises 2,000 images of No Tumor, 1,757 images of Pituitary Tumor, 1,621 images of Glioma, and 1,645 images of Meningioma. Dataset II contains 500 images of No Tumor, 900 images of Pituitary Tumor, 926 images of Glioma, and 937 images of

Meningioma. These images cover a wide spectrum of tumor types and patient demographics and were carefully curated to ensure sufficient quality for subsequent analyses.

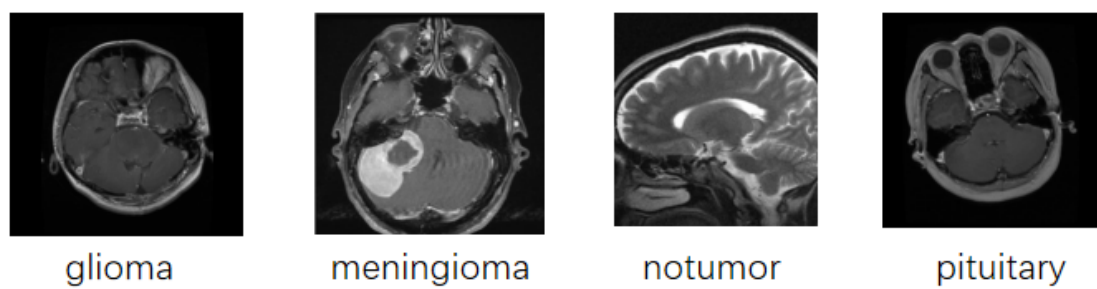


Figure 1. Brain Tumor Types: glioma, meningioma, no tumor, and pituitary.

2.2. S-ResGCN Model

The S-ResGCN model, illustrated in Figure 2, utilizes a standard ResNet50 backbone to extract hierarchical feature representations from input MRI images, effectively capturing low-level textures and edge information. Convolutional Block Attention Modules (CBAM) are integrated after the second and fourth residual blocks to enhance both channel-wise and spatial attention, emphasizing symmetric and discriminative features. Finally, a graph convolutional network (GCN) classification head is applied to the extracted features, incorporating information from both the original and horizontally flipped images to achieve symmetry-aware classification.

Initially, the input MRI images underwent systematic preprocessing and data augmentation to enhance model generalization and reinforce symmetry-aware feature learning. The augmentation pipeline included random rotations, flips, color jittering, and affine transformations. Specifically, each image was randomly rotated within $\pm 30^\circ$, randomly flipped along both horizontal and vertical axes to preserve spatial symmetry, subjected to brightness and contrast adjustments for color jittering, and transformed via translation and scaling. For each original image, five augmented variants were generated, and all images were resized to a uniform dimension of 224×224 pixels.

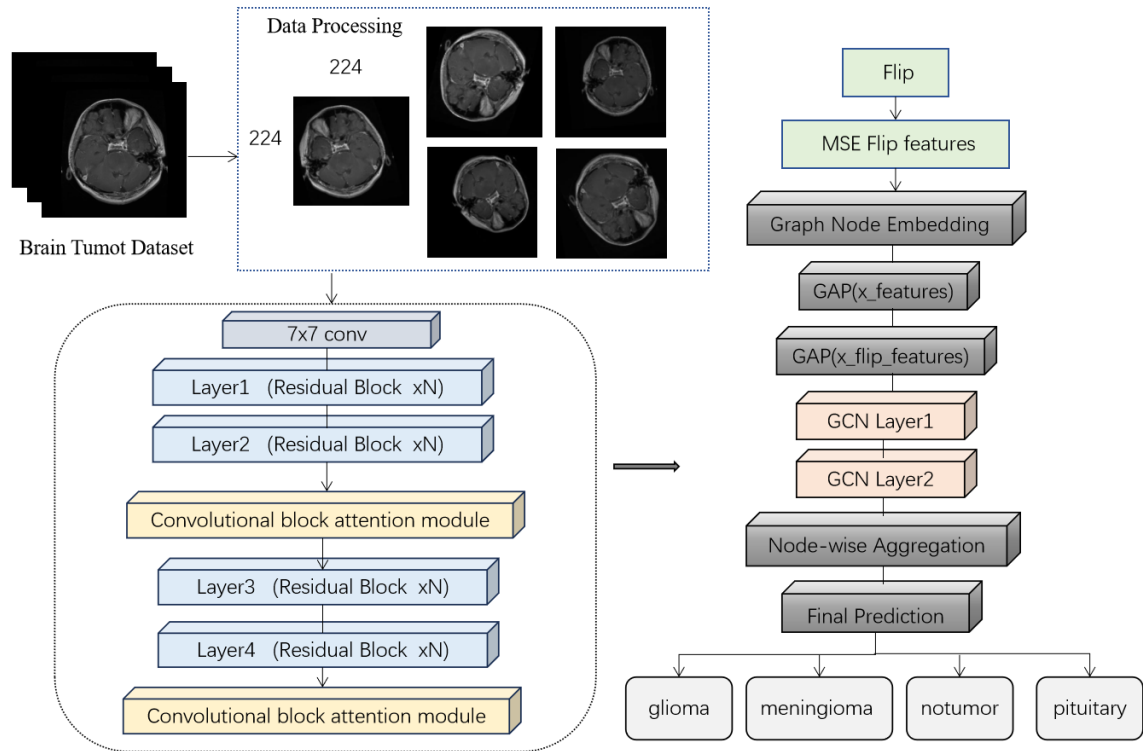


Figure 2. S-ResGCN Model Architecture.

For an input image X_{input} , local convolutional features are first extracted to generate a feature map $X \in \mathbb{R}^{C \times H \times W}$, where C denotes the number of channels, and H and W denote the height and width, respectively. The original 7×7 convolution in the first layer (conv1) followed by batch normalization and ReLU activation, and a 3×3 max-pooling layer produces an initial feature map:

$$X_1 = \text{MaxPool} \left(\text{ReLU} \left(\text{BN}(\text{Conv}_{7 \times 7}(X_{\text{input}})) \right) \right). \quad (1)$$

where $\text{Conv}_{7 \times 7}(\cdot)$ represents a 7×7 convolution operation, $\text{BN}(\cdot)$ denotes batch normalization, $\text{ReLU}(\cdot)$ is the rectified linear unit activation function, and $\text{MaxPool}(\cdot)$ refers to a 3×3 max-pooling operation.

The feature map X_1 is then propagated through the first residual block (layer1), generating:

$$X_2 = \text{Layer}_1(X_1). \quad (2)$$

Next, the second residual block is applied, followed by CBAM to emphasize symmetric and discriminative features:

$$X_3 = \text{CBAM}_2(\text{Layer}_1(X_2)), \quad (3)$$

where Layer_k denotes the k -th residual layer, and CBAM_k represents the attention module in that stage.

The CBAM module sequentially applies channel and spatial attention to emphasize symmetric and discriminative features. As shown in Figure 3, the channel attention mechanism refines the input feature by aggregating spatial information through global average pooling and max pooling, followed by a shared multi-layer perceptron to generate a channel attention map. The channel attention is computed as:

$$A_{\text{channel}} = \sigma \left(W_2 \text{ReLU}(W_1 \cdot \text{GAP}(X_2)) \right), \quad (4)$$

where $\text{GAP}(\cdot)$ represents global average pooling, W_1 and W_2 are learnable weight matrices of the shared multi-layer perceptron, $\sigma(\cdot)$ is the sigmoid activation function, and A_{channel} is the resulting channel attention map.

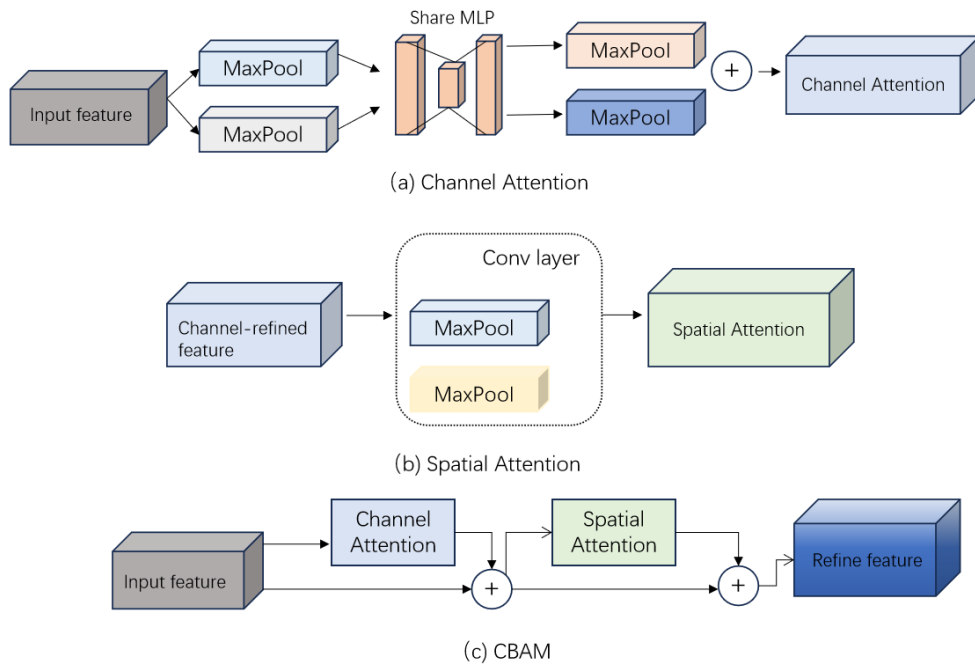


Figure 3. (a) Channel Attention Module. (b) Spatial Attention Module, where the input feature is refined through global pooling and spatial attention. (c) Convolutional Block Attention Module (CBAM), which sequentially applies channel and spatial attention to enhance the input feature.

Spatial attention is computed as:

$$A_{\text{spatial}} = \sigma \left(\text{Conv}([\text{GAP}(X_2), \text{MaxPool}(X_2)]) \right), \quad (5)$$

The CBAM-enhanced feature map is then obtained by:

$$X'_3 = X_3 \cdot A_{\text{channel}} \cdot A_{\text{spatial}} + X_3, \quad (6)$$

where \cdot denotes element-wise multiplication, and X'_3 is the CBAM-enhanced feature map.

Similarly, the feature map is propagated through layer3:

$$X_4 = \text{Layer}_1(X'_3), \quad (7)$$

$$X_5 = \text{CBAM}_4(\text{Layer}_1(X_4)). \quad (8)$$

To reinforce symmetry-aware feature learning, each input image was horizontally flipped to obtain X_{flip} , and its feature map was extracted through the backbone network:

$$X_{\text{flip_features}} = \text{Backbone}(X_{\text{flip}}) \quad (9)$$

The self-paired regularization (SPR) loss enforces symmetry consistency between the original and flipped features, as illustrated in Figure 4. This encourages the network to be sensitive to symmetric structures commonly observed in brain tumors. The SPR loss is computed as:

$$L_{\text{SPR}} = \frac{1}{B} \sum_{b=1}^B \left\| X_5^{(b)} - X_{\text{flip_features}}^{(b)} \right\|_2^2 \quad (10)$$

where B is the batch size, $X_5^{(b)}$ denotes the backbone feature map of the b -th original image (after CBAM), and $X_{\text{flip_features}}^{(b)}$ denotes the corresponding flipped feature map. The squared L2 norm $\|\cdot\|_2^2$ measures the discrepancy between symmetric feature representations.

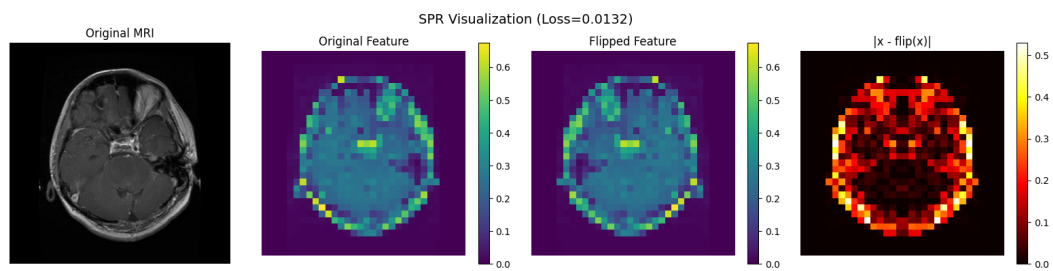


Figure 4. Visualization of the Self-Paired Regularization (SPR) loss. The figure illustrates how SPR enhances symmetry-aware feature learning in brain MRI. The first panel presents the original MRI image, while the second and third panels show the feature maps extracted by the backbone network from the original and horizontally flipped images, respectively. The fourth panel visualizes the absolute difference $|x - \text{flip}(x)|$ between the two feature maps, highlighting regions where symmetry is not fully preserved.

Finally, the feature maps of the original and flipped images are aggregated via Global Average Pooling:

$$\text{Node}_0 = \text{GAP}(X_5), \quad \text{Node}_1 = \text{GAP}(X_{\text{flip_features}}) \quad (11)$$

Graph nodes are constructed as:

$$X_{\text{nodes}} = [\text{Node}_0, \text{Node}_1] \quad (12)$$

The GCN processes node features to produce node-level predictions:

$$H_1 = \text{GCNLayer}_1(X_{\text{nodes}}), \quad H_2 = \text{GCNLayer}_2(H_1) \quad (13)$$

The final prediction aggregates the outputs of original and flipped nodes:

$$\hat{y} = \text{softmax}\left(\frac{1}{2}(H_2[:, 0, :] + H_2[:, 1, :])\right) \quad (14)$$

where Node_0 and Node_1 denote the global average pooled feature vectors of the original and horizontally flipped images, respectively. X_{nodes} is the resulting node matrix, and H_2 is the intermediate node embeddings generated by the first and second GCN layers. $[:, 0, :]$ and $[:, 1, :]$ denote the feature vectors corresponding to the original and horizontally flipped nodes, respectively. Here, “:” indicates all elements along the batch or feature dimension, 0 and 1 select the first (original) and second (flipped) nodes, and the final *softmax* converts the averaged node embeddings into a class probability vector \hat{y} .

2.3. Experiment

In this study, the MRI datasets were divided into training and test sets with a ratio of 4:1 to ensure sufficient diversity for model training and to enhance generalization capability. All experiments were conducted on an NVIDIA GeForce RTX 3090 GPU. CUDA 11.8 and PyTorch 2.7.1+cu118 were used to ensure computational efficiency and reproducibility. A fixed random seed was applied to control experimental variability across runs.

The S-ResGCN model was optimized using the AdamW optimizer with an initial learning rate of 5×10^{-5} and a weight decay of 1×10^{-4} . AdamW extends the conventional Adam optimizer by incorporating weight decay, which mitigates overfitting and improves model generalization. To dynamically adjust the learning rate during training, a *CosineAnnealingLR* scheduler was adopted.

Model performance was systematically evaluated using four standard metrics: Accuracy, Precision, Recall, and F1-score. Accuracy quantifies the overall classification correctness and is defined as:

$$\text{Accuracy} = \frac{TP + TN}{TP + TN + FP + FN} \quad (15)$$

where TP denotes the number of true positives, TN the number of true negatives, FP the number of false positives, and FN the number of false negatives.

Precision measures the proportion of correctly predicted positive samples for a given class:

$$\text{Precision} = \frac{TP}{TP + FP} \quad (16)$$

Recall evaluates the model’s ability to identify actual positive samples:

$$\text{Recall} = \frac{TP}{TP + FN} \quad (17)$$

F1-Score provides a harmonic mean of Precision and Recall, balancing the trade-off between them:

$$\text{F1 Score} = \frac{2 \times (\text{Precision} \times \text{Recall})}{\text{Precision} + \text{Recall}} \quad (18)$$

These metrics collectively provide a multi-dimensional assessment of the model’s classification performance across different tumor categories.

3. Results

3.1. Overall Performance

As shown in Figures 5 and 6, the proposed S-ResGCN model exhibits outstanding performance on the four-class brain tumor classification task across both Dataset I and Dataset II. For all categories—

including meningioma, glioma, no tumor, and pituitary—the model achieved Precision, Recall, and F1-Score values exceeding 98%, with the no tumor category in Dataset II reaching 100%, demonstrating exceptional robustness and highly consistent discriminative capability.

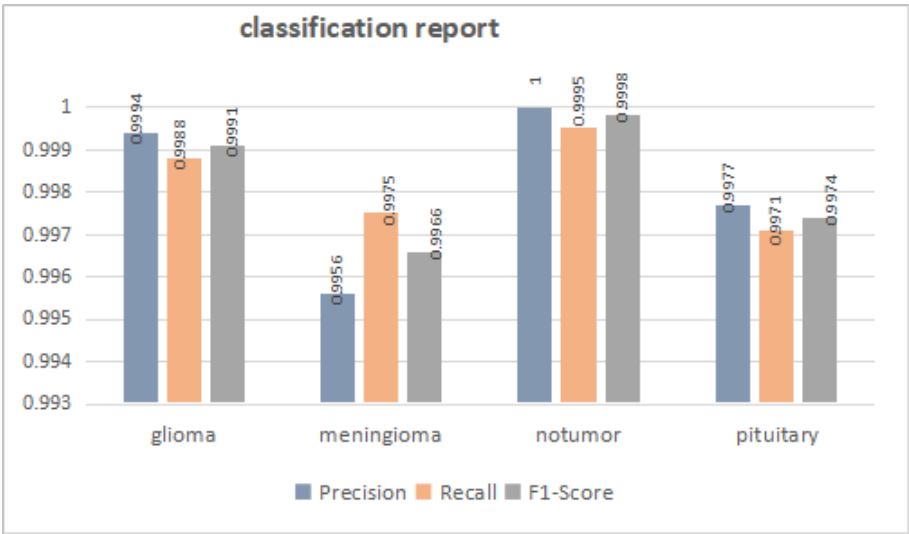


Figure 5. Classification report on the dataset I

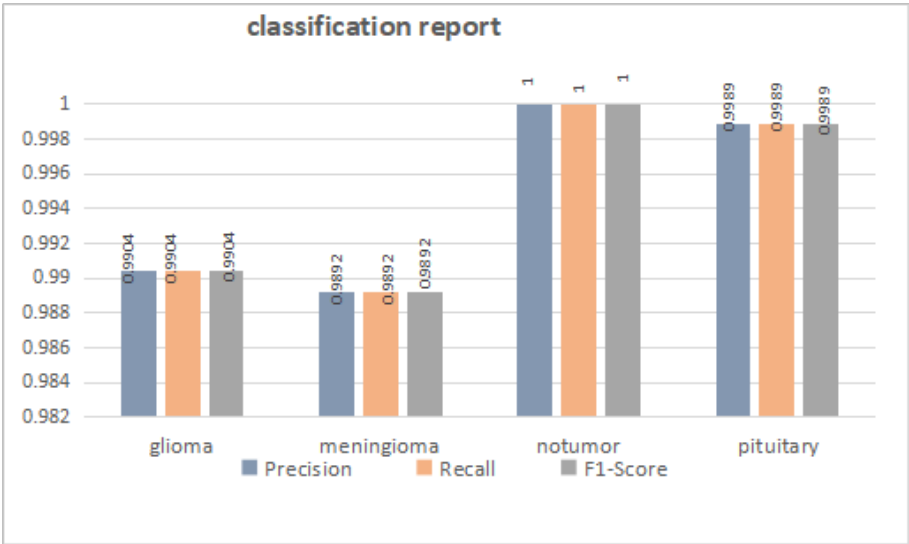


Figure 6. Classification report on the dataset II

The accuracy curves in Figures 7 and 8 indicate that training accuracy increased rapidly during the initial iterations and stabilized above 99%, while validation accuracy converged to 99.83% for Dataset I and 99.37% for Dataset II, reflecting excellent fitting on the training data and superior generalization to unseen samples. The corresponding loss curves show steadily decreasing training loss and smoothly converging validation loss, with no evident signs of overfitting.

Collectively, these results confirm that the S-ResGCN model not only achieves high classification accuracy but also maintains robust stability and generalization, effectively handling MRI images with diverse tumor types and varying levels of complexity.

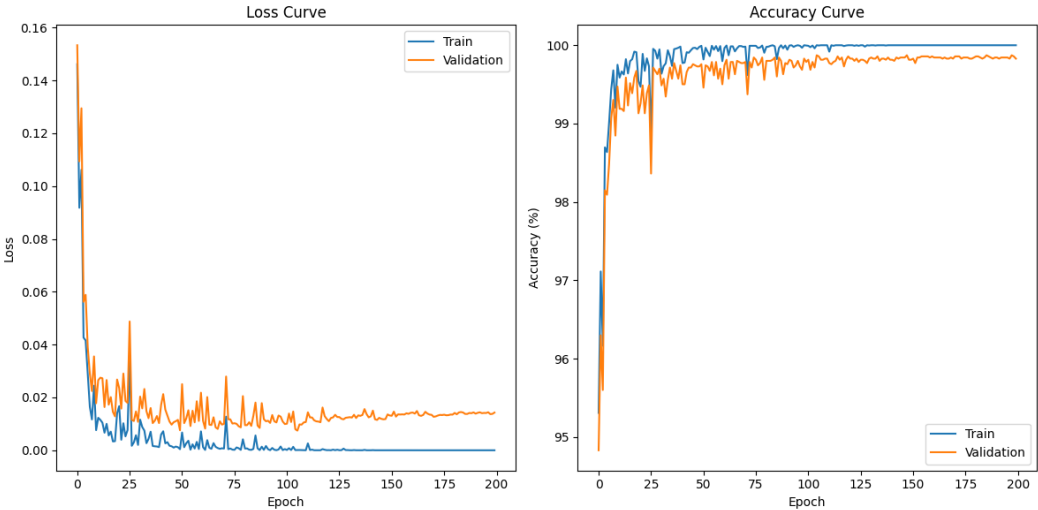


Figure 7. Loss and accuracy curves on the dataset I

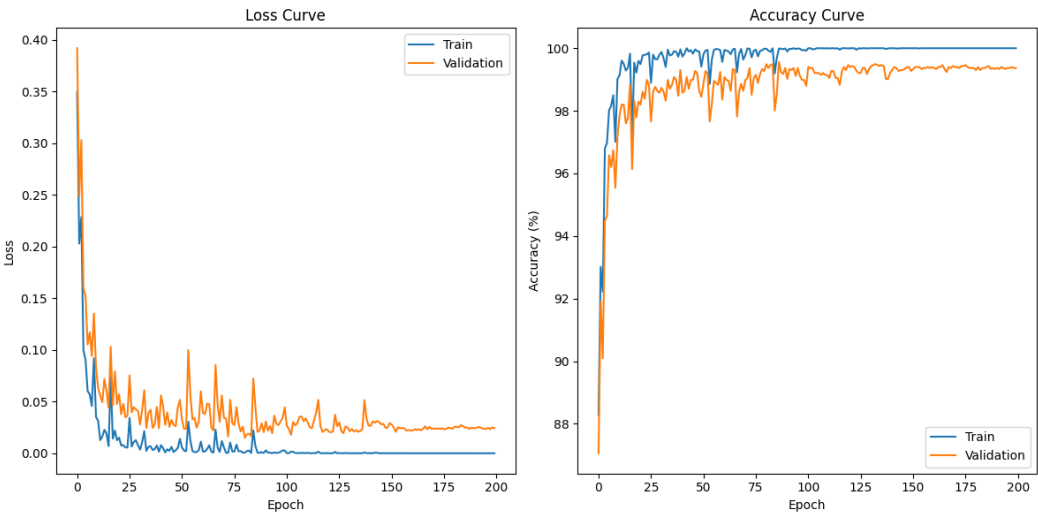


Figure 8. Loss and accuracy curves on the dataset II

3.2. Comparison with Baseline Methods

The proposed S-ResGCN was evaluated on Brain Tumor MRI Dataset I, with its performance summarized in Table 1, and compared against a range of representative models, including lightweight networks, classic CNNs, attention-enhanced architectures, multi-scale networks, and Transformer-based approaches. MobileNetV2 and ResNet-18 achieved moderate accuracies of 84.45% and 86.59%, respectively, while VGG16 improved to 94.97%. The incorporation of attention mechanisms further enhanced performance, as demonstrated by CBAM-CNN with an accuracy of 96.70%. Deeper or multi-scale architectures, such as Inception V3, Pat-GridMask, and Custom CNN, achieved 97%–98% accuracy, whereas the Transformer-based FTVT-132 reached 98.70%.

In contrast, S-ResGCN attained 99.83% across all evaluation metrics, including accuracy, precision, recall, and F1-score, outperforming all baseline methods. This result highlights the effectiveness of hierarchical feature extraction, self-paired regularization, and graph convolutional modeling in capturing fine-grained and symmetric tumor characteristics, which are often overlooked by conventional models.

Table 1. Experimental Results for the Brain Tumor MRI Dataset I.

Methods	Accuracy	Precision	Recall	F1-Score
MobileNetV2 [23]	0.8445	0.8498	0.8445	0.8431
ResNet-18 [23]	0.8659	0.8658	0.8659	0.8635
VGG16 [23]	0.9497	0.9495	0.9497	0.9494
CBAM-CNN [24]	0.9670	0.9675	0.9650	0.9675
Inception V3 [25]	0.9712	0.9797	–	–
Pat-GridMask [26]	0.9774	–	–	0.9775
Custom CNN [27]	0.9809	0.9820	0.9810	0.9815
FTVT-132 [28]	0.9870	0.9870	0.9870	0.9870
S-ResGCN	0.9983	0.9982	0.9982	0.9982

Table 2 presents the classification results on Brain Tumor MRI Dataset II. The proposed S-ResGCN achieved an accuracy of 99.37%, with mean precision, recall, and F1-score all reaching 99.46%, substantially outperforming baseline methods such as Swin Transformer (88.88%), MSCNN (91.20%), HDL2BT (92.13%), and a conventional CNN (93.30%). It also surpassed advanced architectures including EfficientNet-B7 (95.00%), CustomEfficientNet (97.00%), and TLAEN (97.00%), as well as the previously best-performing Innovation CNN (98.20%), achieving nearly 1% higher accuracy while maintaining superior robustness across all metrics. These results indicate that S-ResGCN exhibits remarkable capability in capturing fine-grained features, precise boundary delineation, and minority-class recognition.

The superior performance of S-ResGCN arises from its combination of hierarchical feature extraction, attention-enhanced symmetric feature learning via CBAM, self-paired regularization to enforce symmetry consistency, and a GCN-based head that captures inter-node relationships, collectively enabling more robust and fine-grained brain tumor classification than baseline models.

Table 2. Experimental Results on the Brain Tumor MRI Dataset II.

Methods	Accuracy	Precision	Recall	F1-Score
Swin Transformer [29]	0.8888	0.8600	0.7500	0.8700
MSCNN [30]	0.9120	0.9200	0.9070	0.9100
HDL2BT [31]	0.9213	0.9213	–	–
CNN [32]	0.9330	–	0.9113	–
EfficientNet B7 [33]	0.9500	0.9300	0.9200	0.9300
CustomEfficientNet [34]	0.9700	0.9600	0.9600	0.9600
TLAEN [35]	0.9700	0.9700	0.9700	0.9700
Innovation CNN [36]	0.9820	–	–	–
S-ResGCN	0.9937	0.9946	0.9946	0.9946

3.3. Ablation Studies

An ablation study on the Brain Tumor MRI Dataset II (Table 3) was conducted to evaluate the individual and combined contributions of S-ResGCN’s core components. The baseline ResNet50 backbone achieved an accuracy of 95.73%, indicating limited capability in detecting small or poorly defined lesions. Incorporating the GCN head increased accuracy to 96.99%, demonstrating that graph-based relational modeling effectively strengthens spatial reasoning by aggregating features from both the original and horizontally flipped images. Adding CBAM further improved accuracy to 97.47%, highlighting its capacity to adaptively emphasize informative channels and spatial regions critical for tumor localization. Employing SPR loss alone yielded 96.84% accuracy, confirming that enforcing symmetry consistency enhances robustness to subtle and symmetric tumor structures.

Combining two components resulted in additional performance gains. The combination of CBAM and GCN achieved 98.10% accuracy by effectively integrating attention-guided feature selection with graph-based relational modeling. CBAM combined with SPR reached 97.94% accuracy, leveraging the synergy between attention mechanisms and symmetry-aware regularization to improve lesion

detection. The combination of GCN and SPR achieved 98.42% accuracy, reinforcing both spatial reasoning and symmetry consistency to better discriminate small lesions. The full integration of CBAM, GCN, and SPR achieved the highest accuracy of 99.37%, demonstrating that attention mechanisms, graph-based modeling, and symmetry regularization are complementary, jointly delivering substantial improvements in classification accuracy and the recognition of fine-grained tumor structures.

Table 3. Impact of CBAM, SPR and GCN on Classification Accuracy.

Exp	CBAM	SPR	GCN	Accuracy	Precision	Recall	F1-Score
1				0.9573	0.9504	0.9642	0.9565
2			✓	0.9699	0.9695	0.9729	0.9710
3	✓			0.9747	0.9763	0.9785	0.9772
4		✓		0.9684	0.9635	0.9699	0.9665
5	✓		✓	0.9810	0.9827	0.9828	0.9827
6		✓	✓	0.9794	0.9683	0.9805	0.9740
7	✓	✓		0.9842	0.9847	0.9836	0.9841
8	✓	✓	✓	0.9937	0.9946	0.9946	0.9946

4. Conclusions

In this study, we proposed S-ResGCN, a symmetry-aware framework for brain tumor MRI classification that integrates hierarchical feature extraction, self-paired regularization, and a graph convolutional head. By jointly leveraging original and horizontally flipped images, the model enhances sensitivity to symmetric and discriminative tumor structures, while Convolutional Block Attention Module (CBAM) modules effectively emphasize critical lesion regions. Experiments on two public MRI datasets demonstrated consistently high accuracy, precision, recall, and F1-scores, particularly for complex and symmetric lesions. These findings highlight S-ResGCN’s robustness and its potential as a foundation for automated, symmetry-sensitive diagnostic systems.

In the future, we plan to extend S-ResGCN to multi-modal MRI data and cross-center datasets to improve generalization under diverse imaging conditions. Further exploration of semi-supervised learning may reduce dependence on labeled data, while optimizing computational efficiency could enable real-time clinical deployment. Moreover, incorporating 3D volumetric inputs may enhance its effectiveness for tumor monitoring and treatment planning.

Author Contributions: Yingzhou Bi, Qiuqing Gan, Leigang Huo, Shanrui Liu, and Kairui Xiong contributed to the study conception and design, material preparation, data collection, data analysis, and drafting of the manuscript. All authors have read and agreed to the published version of the manuscript.

Funding: This research was funded by the National Natural Science Foundation of China, grant number 62067007, and the Guangxi Graduate Education and Teaching Reform Project, grant number JGY2023236.

Informed Consent Statement: Not applicable.

Data Availability Statement: The data that support the findings of this study are publicly available. Dataset I, the Brain Tumor MRI Dataset containing 7,023 images, can be accessed at <https://www.kaggle.com/datasets/masoudnickparvar/brain-tumor-mri-dataset>. Dataset II, the Brain Tumor MRI Dataset containing 3,264 images, is available at <https://www.dilitanxianjia.com/13366/>.

Conflicts of Interest: The authors declare no conflicts of interest.

References

1. Katti, G.; Ara, S.A.; Shireen, A. Magnetic resonance imaging (MRI)–A review. *International journal of dental clinics* **2011**, *3*, 65–70.
2. Doi, K. Computer-aided diagnosis in medical imaging: historical review, current status and future potential. *Computerized medical imaging and graphics* **2007**, *31*, 198–211.
3. Jakkula, V. Tutorial on support vector machine (svm). *School of EECS, Washington State University* **2006**, *37*, 3.

4. Wu, J.; Zhu, J.; et al. Review of random forest methods. *Statistics and information BBS* **2011**, *26*, 32–38.
5. Guo, G.; Wang, H.; Bell, D.; Bi, Y.; Greer, K. KNN model-based approach in classification. In Proceedings of the OTM Confederated International Conferences" On the Move to Meaningful Internet Systems". Springer, 2003, pp. 986–996.
6. O'shea, K.; Nash, R. An introduction to convolutional neural networks. *arXiv preprint arXiv:1511.08458* **2015**.
7. Musa, M.N. MRI-based brain tumor classification using resnet-50 and optimized softmax regression. *Jurnal Infotel* **2024**, *16*, 598â–614.
8. Ahmed, G.; Er, M.J.; Fareed, M.M.S.; Zikria, S.; Mahmood, S.; He, J.; Asad, M.; Jilani, S.F.; Aslam, M. Dad-net: Classification of alzheimer's disease using adasyn oversampling technique and optimized neural network. *Molecules* **2022**, *27*, 7085.
9. Nizamli, Y.A.; Filatov, A.Y. Improving transfer learning performance for abnormality detection in brain MRI images using feature optimization techniques. In Proceedings of the 2024 XXVII International Conference on Soft Computing and Measurements (SCM). IEEE, 2024, pp. 432–435.
10. Haq, A.U.; Li, J.P.; Agbley, B.L.Y.; Khan, A.; Khan, I.; Uddin, M.I.; Khan, S. IIMFCBM: Intelligent integrated model for feature extraction and classification of brain tumors using MRI clinical imaging data in IoT-healthcare. *IEEE Journal of Biomedical and Health Informatics* **2022**, *26*, 5004–5012.
11. Wang, M.; Ren, Y.; Lin, Y.; Wang, S. The tightly super 3-extra connectivity and diagnosability of locally twisted cubes. *American Journal of Computational Mathematics* **2017**, *7*, 127–144.
12. Wang, S.; Wang, Y.; Wang, M. Connectivity and matching preclusion for leaf-sort graphs. *Journal of Interconnection Networks* **2019**, *19*, 1940007.
13. Wang, M.; Lin, Y.; Wang, S.; Wang, M. Sufficient conditions for graphs to be maximally 4-restricted edge connected. *Australas. J Comb.* **2018**, *70*, 123–136.
14. Jiang, J.; Wu, L.; Yu, J.; Wang, M.; Kong, H.; Zhang, Z.; Wang, J. Robustness of bilayer railway-aviation transportation network considering discrete cross-layer traffic flow assignment. *Transportation Research Part D: Transport and Environment* **2024**, *127*, 104071.
15. Wang, M.; Xiang, D.; Wang, S. Connectivity and diagnosability of leaf-sort graphs. *Parallel Processing Letters* **2020**, *30*, 2040004.
16. Lin, Y.; Wang, M.; Xu, L.; Zhang, F. The maximum forcing number of a polyomino. *Australas. J. Combin* **2017**, *69*, 306–314.
17. Wang, S.; Wang, M. A Note on the Connectivity of m-Ary n-Dimensional Hypercubes. *Parallel Processing Letters* **2019**, *29*, 1950017.
18. Woo, S.; Park, J.; Lee, J.Y.; Kweon, I.S. Cbam: Convolutional block attention module. In Proceedings of the Proceedings of the European conference on computer vision (ECCV), 2018, pp. 3–19.
19. Rahman, Z.; Zhang, R.; Bhutto, J.A. A symmetrical approach to brain tumor segmentation in MRI using deep learning and threefold attention mechanism. *Symmetry* **2023**, *15*, 1912.
20. Zhang, S.; Tong, H.; Xu, J.; Maciejewski, R. Graph convolutional networks: a comprehensive review. *Computational Social Networks* **2019**, *6*, 1–23.
21. Nickparvar, M. Brain tumor MRI dataset. *Kaggle* **2021**.
22. Sayedgomaa, S. Brain Tumor. Kaggle Notebook, 2022. Available online: <https://www.kaggle.com/code/sayedgomaa/brain-tumor/notebook> (accessed on 21 December 2022).
23. Liu, X.; Wang, Z. Deep learning in medical image classification from mri-based brain tumor images. In Proceedings of the 2024 IEEE 6th International Conference on Power, Intelligent Computing and Systems (ICPICS). IEEE, 2024, pp. 840–844.
24. Binish, M.; Raj, R.S.; Thomas, V. Brain tumor classification using multi-resolution averaged spatial attention features with CBAM and convolutional neural networks. In Proceedings of the 2024 1st International Conference on Trends in Engineering Systems and Technologies (ICTEST). IEEE, 2024, pp. 1–7.
25. Gómez-Guzmán, M.A.; Jiménez-Beristáin, L.; García-Guerrero, E.E.; López-Bonilla, O.R.; Tamayo-Perez, U.J.; Esqueda-Elizondo, J.J.; Palomino-Vizcaino, K.; Inzunza-González, E. Classifying brain tumors on magnetic resonance imaging by using convolutional neural networks. *Electronics* **2023**, *12*, 955.
26. Lee, J.h.; Chae, J.w.; Cho, H.c. Improved classification of different brain tumors in mri scans using patterned-gridmask. *IEEE Access* **2024**, *12*, 40204–40212.
27. Khan, M.A.; Auvee, R.B.Z. Comparative Analysis of Resource-Efficient CNN Architectures for Brain Tumor Classification. In Proceedings of the 2024 27th International Conference on Computer and Information Technology (ICCIT). IEEE, 2024, pp. 639–644.

28. Reddy, C.K.K.; Reddy, P.A.; Janapati, H.; Assiri, B.; Shuaib, M.; Alam, S.; Sheneamer, A. A fine-tuned vision transformer based enhanced multi-class brain tumor classification using MRI scan imagery. *Frontiers in oncology* **2024**, *14*, 1400341.
29. Zahoor, A.; Irfan, M.; Usman, M.; Haider, W.; et al. Brain tumor detection in magnetic resonance images using swin transformer. *Conclusions in Medicine* **2025**, *1*, 1–5.
30. Yazdan, S.A.; Ahmad, R.; Iqbal, N.; Rizwan, A.; Khan, A.N.; Kim, D.H. An efficient multi-scale convolutional neural network based multi-class brain MRI classification for SaMD. *Tomography* **2022**, *8*, 1905–1927.
31. Khan, A.H.; Abbas, S.; Khan, M.A.; Farooq, U.; Khan, W.A.; Siddiqui, S.Y.; Ahmad, A. Intelligent model for brain tumor identification using deep learning. *Applied Computational Intelligence and Soft Computing* **2022**, *2022*, 8104054.
32. Mahmud, M.I.; Mamun, M.; Abdelgawad, A. A deep analysis of brain tumor detection from mr images using deep learning networks. *Algorithms* **2023**, *16*, 176.
33. Wibowo, M.P.; Al Fayyadl, M.B.; Azhar, Y.; Sari, Z.; et al. Classification of brain tumors on mri images using convolutional neural network model efficientnet. *Jurnal RESTI (Rekayasa Sistem dan Teknologi Informasi)* **2022**, *6*, 538–547.
34. Ishaq, A.; Ullah, F.U.M.; Hamandawana, P.; Cho, D.J.; Chung, T.S. Improved EfficientNet architecture for multi-grade brain tumor detection. *Electronics* **2025**, *14*, 710.
35. SHARMA, P.; SHUKLA, A.P. Transfer learning approach using efficientnet architecture for brain tumor classification in Mri images. *Advances and Applications in Mathematical Sciences* **2022**, *21*, 7091–7106.
36. Ramadhani, M.R.; Soesanti, I.; Hidayah, I. Brain Tumor Classification Based on Deep Learning Algorithms. In Proceedings of the 2024 4th International Conference on Electronic and Electrical Engineering and Intelligent System (ICE3IS). IEEE, 2024, pp. 81–86.

Disclaimer/Publisher's Note: The statements, opinions and data contained in all publications are solely those of the individual author(s) and contributor(s) and not of MDPI and/or the editor(s). MDPI and/or the editor(s) disclaim responsibility for any injury to people or property resulting from any ideas, methods, instructions or products referred to in the content.